JACS
JOURNAL OF THE AMERICAN CHEMICAL SOCIETY
Article
pubs.acs.org/JACS

Computational Insight into the Initial Steps of the Mars–van Krevelen Mechanism: Electron Transfer and Surface Defects in the Reduction of Polyoxometalates

Irena Efremenko and Ronny Neumann*

Department of Organic Chemistry, Weizmann Institute of Science, Rehovot 76100, Israel

Supporting Information

ABSTRACT: Metal oxides as a rule oxidize and oxygenate substrates via the Mars–van Krevelen mechanism. A well-defined α-Keggin polyoxometalate, $H_5PV_2Mo_{10}O_{40}$, can be viewed as an analogue of discrete structure that reacts via the Mars–van Krevelen mechanism both in solution and in the gas phase. Guided by previous experimental observations, we have studied the key intermediates on the reaction pathways of its reduction by various compounds using high-level DFT calculations. These redox reactions of polyoxometalates require protons, and thus such complexes were explicitly considered. First, the energetics of outer-sphere proton and electron transfer as well as coupled proton and electron transfer were calculated for seven substrates. This was followed by identification of possible key intermediates on the subsequent reaction pathways that feature displacement of the metal atom from the Keggin structure and coordinatively unsaturated sites on the $H_5PV_2Mo_{10}O_{40}$ surface. Such *metal defects* are favored at vanadium sites. For strong reducing agents the initial outer-sphere electron transfer, alone or possibly coupled with proton transfer, facilitates formation of metal defects. Subsequent coordination allows for formation of reactive ensembles on the catalyst surface, for which the selective oxygen-transfer step becomes feasible. Weak reducing agents do not facilitate defect formation by outer-sphere electron and/or proton transfers, and thus formation of metal defect structures prior to the substrate activation is suggested as an initial step. Calculated geometries and energies of metal defect structures support experimentally observed intermediates and demonstrate the complex nature of the Mars–van Krevelen mechanism.

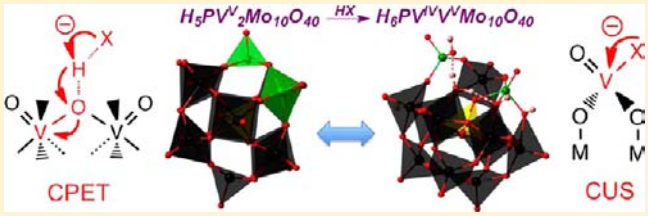

INTRODUCTION

Many heterogeneous oxidation reactions catalyzed by metal oxides have been shown to react via the Mars–van Krevelen mechanism. In such reactions, substrates are dehydrogenated or oxygenated by oxygen atoms from the catalyst bulk, and then the reduced catalyst is reoxidized by molecular oxygen. This spatiotemporal separation between the substrate oxidation and the catalyst regeneration is responsible for high selectivity of such reactions. In view of the enormous significance of selectivity in industrially important processes, substantial efforts have been devoted to searching for the preferential structure of active and selective sites on the catalyst surface at reaction conditions. Polyoxometalates, a class of molecular inorganic compounds with a metal oxide surface structure,[1] present a useful example of site isolation and often provide important mechanistic insights regarding reactions on oxide surfaces in both homogeneous and heterogeneous reaction media.[2] Like bulk metal oxides, acidic phosphomolybdates and phosphovanadomolybdates of the α-Keggin structure, $H_{3+x}PV_xMo_{12-x}O_{40}$, with x = 0, 1, 2, are active, selective, and environmentally friendly homogeneous catalysts that operate at ambient conditions and also use molecular oxygen as the terminal oxidant.[3] They usually react via the Mars–van Krevelen mechanism, where substrates are selectively oxygenated by an oxygen atom from the polyoxometalate lattice.[4] For several reactions such as oxidation of arenes, alkylarenes, and sulfides, the *outer-sphere* reduction of the polyoxometalate has been shown to precede oxygen transfer.[4d−f] In these cases, the electron transfer (ET) can be accompanied by proton transfer (PT) that can occur before, after, or in concert with (CPET) the ET (Scheme 1).

Some other studies indicate that chemisorption and *inner-sphere* activation of a reductant presents a key stage of the interaction.[5,6] In this case the Keggin structures are surmised to

Scheme 1. Initial Reactants and Products of Stepwise Proton Transfer (PT), Electron Transfer (ET), and Concerted Proton and Electron Transfer (CPET)

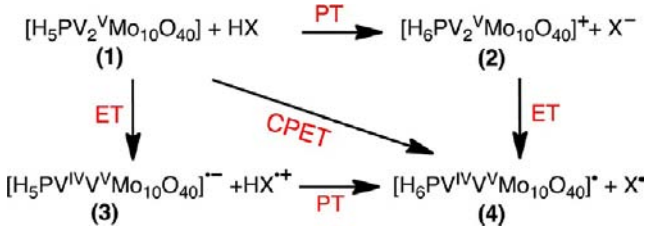

Received: August 30, 2012
Published: December 4, 2012

   dx.doi.org/10.1021/ja308625q | J. Am. Chem. Soc. 2012, 134, 20669–20680

be the precursors of the active catalysts, while the working form involves partial decomposition of the polyoxometalate into a metastable defect structure,[7] which possesses coordinatively unsaturated metal sites (CUSs). Moreover, even though outer-sphere electron transfer has been observed as the initial step of a substrate−polyoxometalate interaction, substrate coordination on metal sites of the catalyst appear to be essential for subsequent *selective* oxygenation reactions. Indeed, defect structures with displacement of vanadium reaction centers from the polyoxometalate were observed as intermediates in the reduction of $H_5PV_2Mo_{10}O_{40}$ by methanol using *in situ* molecular spectroscopy and by various electron paramagnetic resonance (EPR) spectroscopic methods during the reduction of $H_5PV_2Mo_{10}O_{40}$ with several reducing agents.[8] However, the detailed structure and mechanism of formation of CUSs on metal oxide surfaces in general and on polyoxometalates in particular, especially as related to redox activity, are still poorly understood.

Thus, a rational interpretation of possible reaction mechanisms requires accurate energetic data both on the initial outer-sphere reactions shown in Scheme 1 and on the structure, stability, and catalytic behavior of the CUSs. Since the energetics and structure strongly depend on the positioning of the protons' counterions on the polyoxometalate surface,[9] we recently studied the geometry, electronic structure, and energetics of protonated $H_{3+x}PV_xMo_{12-x}O_{40}$ using high-level density functional theory (DFT).[10] Now we have extended our study to calculations of their cationic (**2**) and reduced (**3** ,**4**) forms, Scheme 1, using the (1,2) isomer of $H_5PV_2Mo_{10}O_{40}$ as a representative compound because it has all types of possible nucleophilic sites and has been shown to be reactive in oxygen-transfer reactions.[8] In order to get insight into the initial stages of the outer-sphere, Scheme 1, and inner-sphere interactions of substrates with $H_5PV_2Mo_{10}O_{40}$, we considered the intact α-Keggin structure as well as hypothetical defect structures in which one, two, or three metal−oxygen bonds around the same metal atom are broken. These defect structures are similar but not identical to the well-known lacunary polyoxometalate structures, since the metal atoms remain connected to the defect site, whereas in the lacunary structures one or more addenda atoms and their attendant oxide ions are completely removed. They are also related to the defect structures that feature oxygen vacancies[10,11a,b] or expansion of two adjacent five-coordinated metal atoms, the reactive forms of polyoxometalates that were first addressed theoretically by Rustad, Loring, and Casey.[11c−f]

The present work is devoted to discussion of the three topics. First, the thermodynamics of the outer-sphere ET, PT, and CPET reactions with various substrates, previously studied experimentally, are considered on the basis of the accurate energies of intact complexes **1**−**4**. Then, the structure and energetics of the *metal* defects in complexes **1**−**4** in the absence and in the presence of additional water and HI ligands are addressed in relation to protonation of bimetallic polyoxometalates. Finally, the results presented in these two subsections are applied to study the mechanisms of several redox reactions of $H_5PV_2Mo_{10}O_{40}$ and possible intermediates along the reaction pathways. For modeling of both outer-sphere and inner-sphere interactions, we chose several substrates for which reliable experimental data are available.[4d,f,g,5,8a,32]

COMPUTATIONAL METHODS

All computations were done using the Gaussian 03 and Gaussian 09 packages.[12] Geometry optimizations and evaluation of harmonic frequencies were performed using DFT,[13] employing the nonempirical GGA density functional PBE[14] combined with the PC1 basis set, which is a combination of the Jensen's polarization-consistent pc-1 basis set[15] for the main group elements and the relativistic energy-consistent pseudopotential (RECP) basis set SDD[16] for transition metals, with added *f*-type polarization exponents taken as the geometric average of the two f-exponents given by Martin and Sundermann.[17] This combination is of double-ζ plus polarization quality. The density fitting (DF) approach[18] for treatment of the two-electron integrals was applied in these calculations. The accuracy of the computational method in prediction of geometry of polyoxometalates was validated in our previous work.[19] All the structures discussed in the present work present minima on the corresponding potential energy surfaces, as confirmed by the absence of imaginary frequencies. Single-point calculations on optimized geometries were performed using the empirical hybrid meta-GGA functional M06[20] combined with the same basis set (M06/PC1) and using the same pure GGA functional combined with the larger AUG-PC1 basis set and the DF approach (DF-PBE/AUG-PC1). The AUG-PC1 basis set presents a combination of the aug-pc-1 basis set on the main group elements[15,21] and the SDD basis set with added *f* basis functions on transition metals. The final level of theory applied in the present work is $E_e = E$[DF-PBE/AUG-PC1] − E[DF-PBE/PC1] + E[M06/PC1].

Bulk solvent effects of acetonitrile or water media have been taken into account via the self-consistent reaction field (SCRF) method, using the continuum solvation model COSMO (conductor-like screening model) as implemented in Gaussian 03.[22] The SCRF calculations were performed at the M06/PC1 level. Dispersion interactions within the computed structures were taken into account by adding an empirical dispersion correction term, as proposed by Schwabe and Grimme,[23] with a value $s_6 = 0.25$, as suggested by Karton et al. for the M06 functional.[24] The van der Waals effects are quite significant for reactions with substantial changes in geometry[25] and may also be important for the cases when atoms leave their positions on the polyoxometalate surface and become bound to the remainder of the molecule by only one or two bonds. On the other hand, application of both solvation and dispersion corrections is not fully balanced.[26] Although dispersion interactions between solvent and solute are properly accounted for in the COSMO model,[27] we suppose that bond dissociation energies obtained using this combined approach are slightly overestimated. Unless stated otherwise, energetic data are presented as free energies (ΔG) at 298 K in acetonitrile solution and include dispersion correction. It is important for the present study that in some recent publications it was reported that pure GGA functionals tend to overestimate the stability of lower coordinated complexes.[28] This problem is resolved when hybrid density functionals are used and solvation corrections are accounted for.[28c]

It is not possible to consider all unique coordination positions for all hydrogen atoms on the surface of low-symmetry defect $H_5PV_2Mo_{10}O_{40}$ structures. Thus, we started from the most stable $H_5PV^{V}_{2}Mo_{10}O_{40}$ isomers found in our previous work[10] and considered possible movement of protons to and from the defect site, paying less attention to searching for their most stable positions on the nondefect sites. At least five isomers with protons in different positions were considered for each defect structure. One or two representative defect structures were then chosen to study their interaction with the various substrates.

RESULTS AND DISCUSSION

1. Outer-Sphere Electron and Proton Transfers. The mechanism of coupled proton and electron transfer is actively debated in the current literature.[29] Although the propensity for PT and ET of electron donors can be characterized by their acidity and ionization potential, and the likelihood of hydrogen atom donation for many known CPET reagents is also well

dx.doi.org/10.1021/ja308625q | J. Am. Chem. Soc. 2012, 134, 20669−20680

documented,[30] the distinction between concerted and sequential mechanisms is usually difficult because of the absence of the corresponding data on the oxidant itself.[31] Explicit consideration of protons in complexes **1**−**4** enabled accurate calculation of their energies. This then allowed us to calculate the thermodynamics of the outer-sphere reactions shown in Scheme 1 for several known reducing substrates, Table 1.

Table 1. Calculated ΔG_{298} (kcal/mol) for the Outer-Sphere Interaction of $H_5PV^V_2Mo_{10}O_{40}$ (1) with Selected Substrates (HX)

	PT (**1**→**2**)	ET (**1**→**3**)	CPET (**1**→**4**)
	Gas Phase		
HI	118.9	119.8	9.3
anthracene	184.4	44.4	42.4
xanthene	158.2	54.0	4.5
thioanisole	182.5	60.5	26.5
ascorbic acid	123.1	83.5	7.6
methanol	178.9	127.7	28.5
1-butanol	174.6	112.5	26.0
	Acetonitrile Solution		
HI	17.5	31.2	6.5
anthracene	96.7	−12.9	39.2
xanthene	76.3	−3.8	1.1
thioanisole	92.4	−2.8	23.9
ascorbic acid	39.4	11.4	4.9
methanol	72.0	38.2	24.9
1-butanol	72.5	35.1	22.6

First and foremost these data show that, in the gas phase, both sequential reaction pathways are thermodynamically forbidden. The concerted transfer is readily accessible at 298 K for HI, xanthene, and ascorbic acid, whereas for thioanisole, anthracene, and alcohols CPET is possible only at higher temperatures. In a polar solution ET and PT products are strongly stabilized, so ET becomes spontaneous for anthracene, xanthene, and thioanisole. It represents the preferential initial reaction step for these substrates, although for xanthene the product of CPET is only 5 kcal/mol higher in energy. Other initial electron- or/and proton-transfer steps remain endergonic in polar solution, but the CPET reaction step is easily accessible for HI and ascorbic acid. These energetic data are consistent with experimental observations such as the formation of thioanisole and anthracene cation radicals,[4d,f] the high reactivity of HI,[32] and the more elevated temperatures needed for oxidative C−H and C−C bond cleavage in methanol[5] and in higher primary alcohols,[4g] respectively. However, subsequent selective transformation of the intermediates into final oxidized or oxygenated products seems to require their coordination to the metal sites for most of the substrates. Thus, in order to model the further inner-sphere catalytic reactions, we first considered different CUSs that could be present on the surface of complexes **1**−**4** under reaction conditions.

2. Surface Defects. Polyoxoanions with Keggin structure $XM_{12}O_{40}^{n-}$ are formed by d^0 and d^1 metals, usually Mo, W, or V and their mixtures weakly bound to a tetrahedral heteroatom oxide such as SiO_4^{4-} or PO_4^{3-}. Similar to bulk metal oxides, they feature three types of surface O-atoms (Figure 1a): terminal atoms (O_t), corner- (O_c) and edge-sharing (O_e) bridge atoms, as well as inner O-atoms of the central tetrahedron (not shown in the Figure). In phosphovanadomolybdates the oxygen atoms bound to one (O^V) or two (O^{VV}) vanadium atoms are not equivalent to the atoms having only Mo−O bonds; different types of surface oxygen atoms show different protonation patterns and consequently different chemical behavior.

Available theoretical results indicate that the protons are localized on the bridging corner- (O_c) and edge-sharing (O_e) oxygen atoms, Figure 1a. They are located as distant from each other as possible in $H_3PW_{12}O_{40}$ and $H_3Mo_{12}O_{40}$.[10,11] However, in the vanadium-substituted α-Keggin polyoxometalates, up to three protons are bound to O_c^V and O_e^V sites around the same vanadium atom in the ground-state isomers.[10] This results in strong destabilization of oxo−vanadium bonding to the remainder of the complex and could eventually lead to cleavage of up to three metal−O^V bonds around the vanadium atom. In contrast to oxygen vacancies, for which the loss of the metal−oxygen bonds is compensated by strengthening of the remaining bonds,[10,11] these defects are characterized by the *displacement of the metal atom* from its original position, so that it becomes bound to the remainder of the Keggin structure by either three (***def***$_3$), two (***def***$_2$), or one (***def***$_1$) bond. Typical geometries of such defect species are shown in Figure 1b−d together with characteristic distances of the displaced V_1 atom from the central P atom.[33] All the structures are stabilized by hydrogen bonds, which determine the variation in the P−V_1 distances for each structure.

The defect structures ***def***$_3$ with only one broken metal−oxygen bond yield a distorted square pyramidal configuration around the displaced V_1 atom, Figure 1b, and resemble the defect structures with expansion of two five-coordinated metal atoms found previously as intermediates in oxygen exchange reactions in substituted (Ge,Ga,Al)-Al_{12} ε-Keggin polyoxocations.[11c−f] They are stabilized by the O_t−H hydrogen bond, and, due to a similar geometry, they readily transform back to the original α-Keggin structure. We were unsuccessful in optimizing the geometry of ***def***$_3$ structures with a displaced molybdenum atom. The energy cost for breaking double-protonated M−OH_2 bonds, as in Figure 1b, is 7−12 kcal/mol smaller than that for M−OH bonds. Due to relatively high energy and restricted steric conditions, the ***def***$_3$ structure seems to be an intermediate between the intact α-Keggin structure and more open defects rather than an active form of the catalyst.

In the most stable defect structures ***def***$_2$, two metal−oxygen bonds are broken in such a way that the displaced vanadium atom (V_1 in Figure 1c) is ligated to four oxygen atoms. One of the broken bonds leaves a CUS on the adjacent metal atom, preferentially on vanadium. The second dangling bond is located on the oxygen atom (O* in Figure 1c) and prefers to be doubly protonated. The remaining protons are localized in the vicinity of the defect site and stabilize the ***def***$_2$ isomers by hydrogen bonding. The ***def***$_2$ complexes with a displaced molybdenum atom are by 12−19 kcal/mol less stable than the analogous vanadium defect structures. The ***def***$_2$ complexes are sterically more open and also more stable than defect structures with an oxygen vacancy, especially in the presence of a coordinated water molecule, thus presenting more probable intermediates in chemical reactions (*vide infra*).

The defect structures ***def***$_1$, in which the displaced metal atom is bound to the remainder of the polyoxometalate core by only one bond, have an open geometry resembling classical metal complexes. Numerous reported results may be associated with the formation of ***def***$_1$ structures under reaction conditions.[5,7,34]

dx.doi.org/10.1021/ja308625q | J. Am. Chem. Soc. 2012, 134, 20669−20680

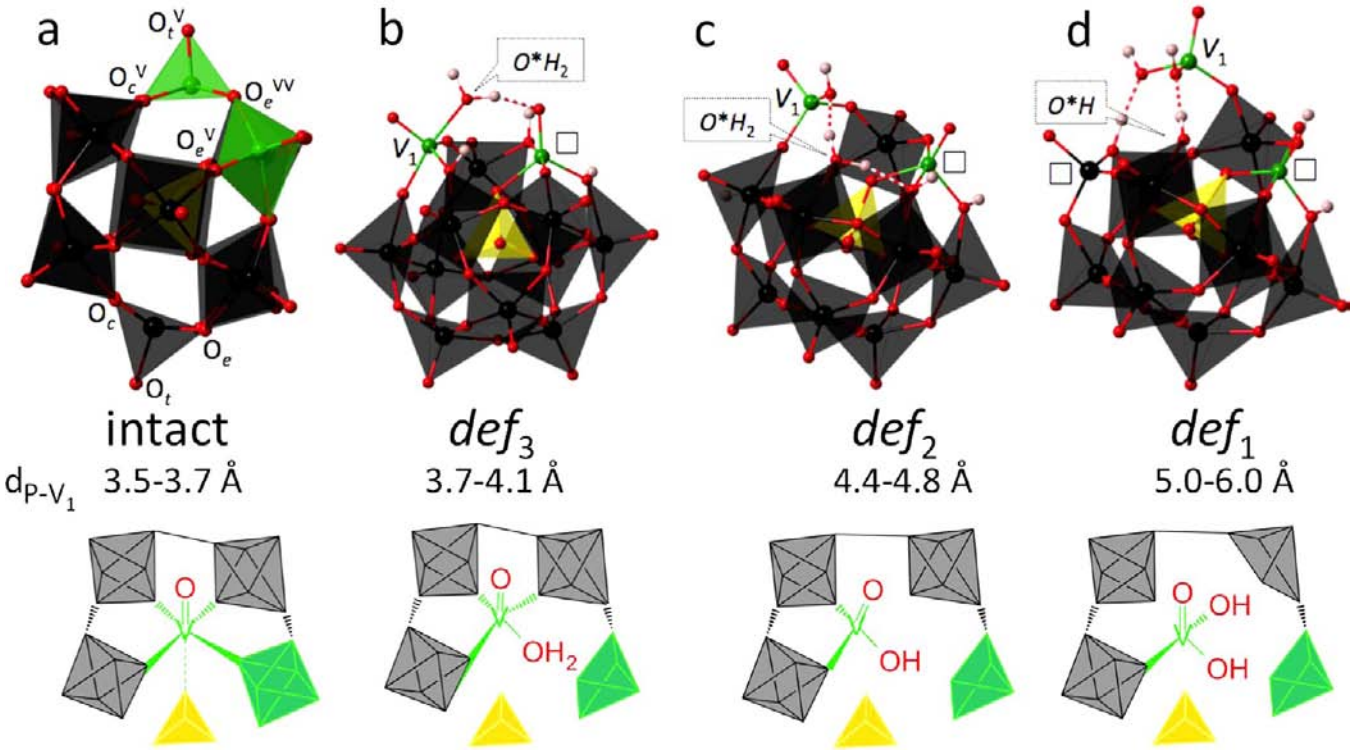

Figure 1. Intact structure of the (1,2) isomer of α-$PV_2Mo_{10}O_{40}^{5-}$ with notations for distinct types of surface oxygen atoms (a). Typical metal defects with vanadium atom V_1 bound to the Keggin structure by three (b), two (c), or one (d) bridging O-atom. Hereinafter, coordinatively saturated sites are shown in polyhedral model while unsaturated sites are shown as balls and sticks. CUSs inside Keggin structure are marked by hollow squares; dangling bonds on oxygen atoms are marked by stars, and their protonation state is indicated. For clarity, the ligand environment of the vanadium atom V_1 in these structures is schematically shown in the bottom panel. Color scheme applied hereinafter: P, yellow; O, red; V, green; Mo, black; H, pink; C, brown; S, orange.

Moreover, a displaced VO_x unit was found as a product of $H_5PV_2Mo_{10}O_{40}$ reduction, where the P−V distance was estimated to be greater than 5 Å.[8] In the most stable ***def*$_1$** structures, breaking of three bridging metal−oxygen bonds results in a distorted tetrahedral ligand environment around the displaced vanadium atom (V_1 in Figure 1d), CUSs on two other metal atoms, and one dangling bond on the oxygen atom (O* in Figure 1d). Coordination of additional ligands, such as a water molecule or dissociated HI, saturates the dangling bonds on metal atoms and thus significantly stabilizes ***def*$_1$** structures, Table 2.

The results presented above show that formation of metal defects is related to the ability to form both octahedral and tetrahedral metal−oxo complexes. The calculations also indicate that tetrahedral coordination around vanadium atoms is energetically beneficial, in contrast to molybdenum atoms, which prefer an octahedral ligand environment. The reason for this behavior can be traced back to the electronic structure of the two metals. Although both molybdenum(VI) and vanadium(V) have a formal d^0 electronic configuration, in the crystal field of σ- and π-donor ligands the occupied molecular orbitals have non-negligible contributions of valence d electrons of the metals.[10] Similar bridging metal−oxygen bond lengths in conjunction with the significant difference in valence d shell orbital radii of vanadium and molybdenum, 0.48 and 0.73 Å, respectively,[35] lead to a much better overlap between oxygen p_π and metal d_π orbitals and a much higher gap between the resulting π and π^* molecular orbitals for the diffuse orbitals of molybdenum than for the more localized orbitals of vanadium. As a result, strongly antibonding t_{2g} (π^*) orbitals lie above the HOMO level in the *octahedral* α-Keggin molybdenum(VI) complexes, whereas in analogous vanadium(V) complexes t_{2g} orbitals have less antibonding character and hence are occupied, Figure 2a. Preferential protonation of the nucleophilic sites around the vanadium atoms accompanied by weakness of vanadium−oxygen bridging bonds is one of the consequences of this difference in the electronic structure of the two metals.

Table 2. Relative Energies of the Defect Structures 1−4 (ΔG_{298}, kcal/mol) with Respect to the Intact Ground-State Isomers in the Absence and in the Presence of an Additional Water Molecule

	1	2	3	4	1 + HI
			Gas Phase		
O-vacancy	28.76	27.66	23.26	23.19	9.32
***def*$_3$**	25.75	27.47	23.00	23.81	26.26
***def*$_2$**	20.37	18.24	22.23	18.13	3.21
***def*$_1$**	47.48	40.01	35.62	44.87	20.02
***def*$_3$·H_2O**	23.11	20.70	26.40	26.42	
***def*$_2$·H_2O**	4.71	7.69	11.97	12.31	4.93
***def*$_1$·H_2O**	20.68	17.60	23.52	26.61	11.38
			Acetonitrile Solution		
O-vacancy	19.29	21.56	15.18	16.45	19.29
***def*$_3$**	25.03	27.48	20.18	23.98	27.92
***def*$_2$**	23.89	17.99	23.54	19.18	5.09
***def*$_1$**	45.81	42.74	32.49	45.84	25.98
***def*$_3$·H_2O**	25.64	19.38	26.63	20.26	
***def*$_2$·H_2O**	9.97	8.86	12.21	11.79	10.94
***def*$_1$·H_2O**	26.95	27.17	26.72	29.29	15.53

dx.doi.org/10.1021/ja308625q | J. Am. Chem. Soc. 2012, 134, 20669−20680

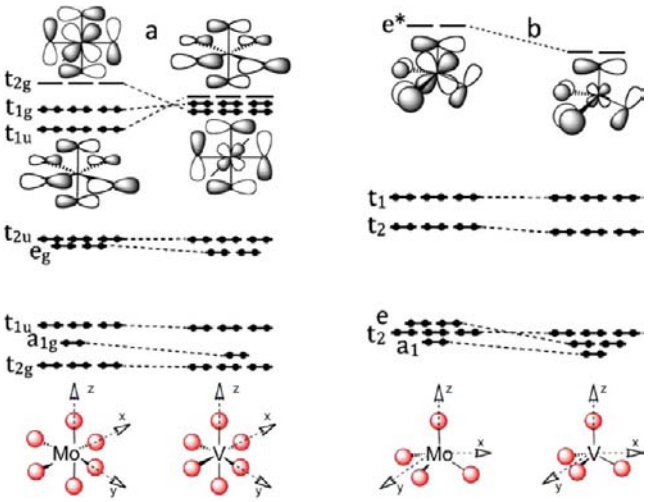

Figure 2. Qualitative representation of the relative energy levels of molybdenum(VI) and vanadium(V) complexes in the octahedral (a) and tetrahedral (b) crystal field of σ- and π-donor ligands.

The favored formation of a CUS on vanadium represents another consequence of having the same electronic structural feature. Indeed, in the *tetrahedral* crystal field of σ- and π-donor ligands, the e_g (π^*) orbitals become empty for vanadium(V). These orbitals represent the LUMO of the complex and lie much lower in energy than the corresponding orbital in the molybdenum(VI) complex, Figure 2b. Therefore, vanadium atoms in phosphovanadomolybdates possess a better structural accessibility and higher electron-withdrawing propensity compared to molybdenum atoms.

3. Inner-Sphere Coordination of Reactants and Products. With the information obtained on the geometric and electronic structure of the CUSs, we can now consider the possible role of the defect structures in typical reactions of $H_5PV_2Mo_{10}O_{40}$. In order to provide a plausible picture of which intermediates can be involved in the initial stages of each particular process, the following analysis is based on thermodynamic stability of several possible intermediates along the reaction pathways. Kinetic barriers of these reactions could be estimated, to a first approximation, as proportional to the difference in the heat effects of the reactions, according to the well-known Bell–Evans–Polanyi principle.

Oxygen Isotope Exchange. Oxygen isotope exchange with labeled water is one of the simplest reactions. Although it is closely associated with the Mars–van Krevelen mechanism, it is not a redox process. Hence, the most important intermediates to be considered on this reaction pathway could be inferred from geometries and energies of various defect isomers of complex **1**. Formation of an oxygen vacancy is often assumed to be a first step of this reaction in acidic media.[36] Formation of ***def***$_3$ structures with an additional water molecule coordinated at the only CUS gives another possible intermediate. Similar structures were addressed in a DFT study of oxygen exchange in (Ge,Ga,Al)-Al_{12}[11c–f] and in $Ti_nNb_{(10-n)}$[37] polyoxometalates. Our calculations show that the relevant ***def***$_2$***·H$_2$O*** structures are by far more stable than the other defect structures. The energy costs for the formation of an oxygen vacancy and ***def***$_3$***·H$_2$O***, ***def***$_2$***·H$_2$O***, and ***def***$_1$***·H$_2$O*** complexes are 19.05, 25.26, 9.43, and 26.39 kcal/mol, respectively, in water at room temperature. That sets the defect structures ***def***$_2$ as the most probable key intermediates in oxygen exchange of $H_5PV_2Mo_{10}O_{40}$. The low energy of this intermediate is in accord with the experimentally observed high rate of the reaction. Feasible proton-assisted exchange between different kinds of oxygen atoms in these structures is also consistent with the fact that not only bridging but also terminal oxygen atoms are involved in exchange with labeled water.[4e,38]

Reduction of Polyoxometalates. Reduction of polyoxometalates can start by outer-sphere PT, ET, or CPET (*vide supra*) reactions. Probable key intermediates along the subsequent stepwise transformation of the ET and CPET products into the defect structures ***def***$_3$ and ***def***$_2$ of complexes **3** and **4** followed by coordination of the activated substrate with formation of the triplet (***def***$_2$-XH(T) and ***def***$_2$-X(T), respectively) and singlet (***def***$_2$-XH and ***def***$_2$-X) complexes are shown on the same energy scale in Figures 3 and 4, together with the calculated

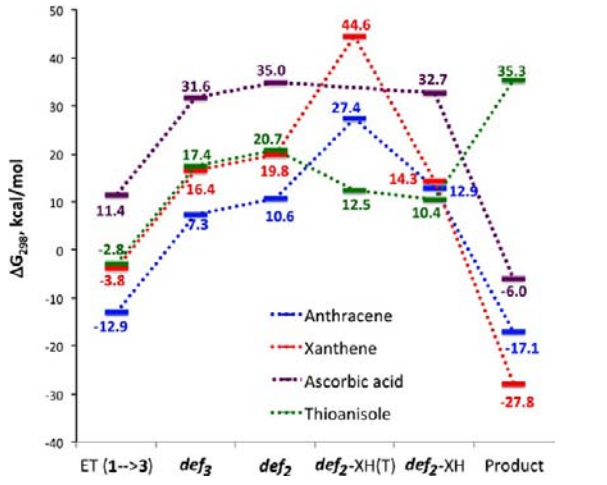

Figure 3. Relative stabilities in acetonitrile of key intermediates and total thermodynamic effect of $H_5PV^V_2Mo_{10}O_{40}$ reduction according to reactions (2a), (3), (4), and (5b) with outer-sphere ET as an initial step. Mutual transformations of the intermediates are not considered; the lines are drawn to guide the eye. The individual reactants $H_5PV_2Mo_{10}O_{40}$ and the substrate are taken as the reference energy point. See text for details.

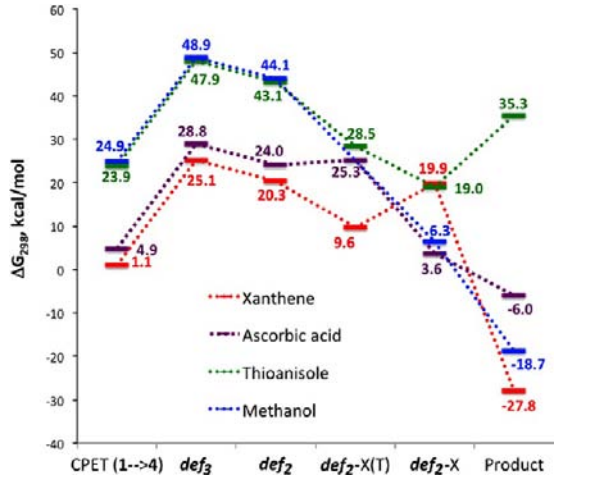

Figure 4. Relative stabilities in acetonitrile of key intermediates and total thermodynamic effect of $H_5PV^V_2Mo_{10}O_{40}$ reduction according to reactions (1a), (2a), (4), and (5b) with outer-sphere CPET as an initial step. For more details, see caption to Figure 3.

dx.doi.org/10.1021/ja308625q | J. Am. Chem. Soc. 2012, 134, 20669–20680

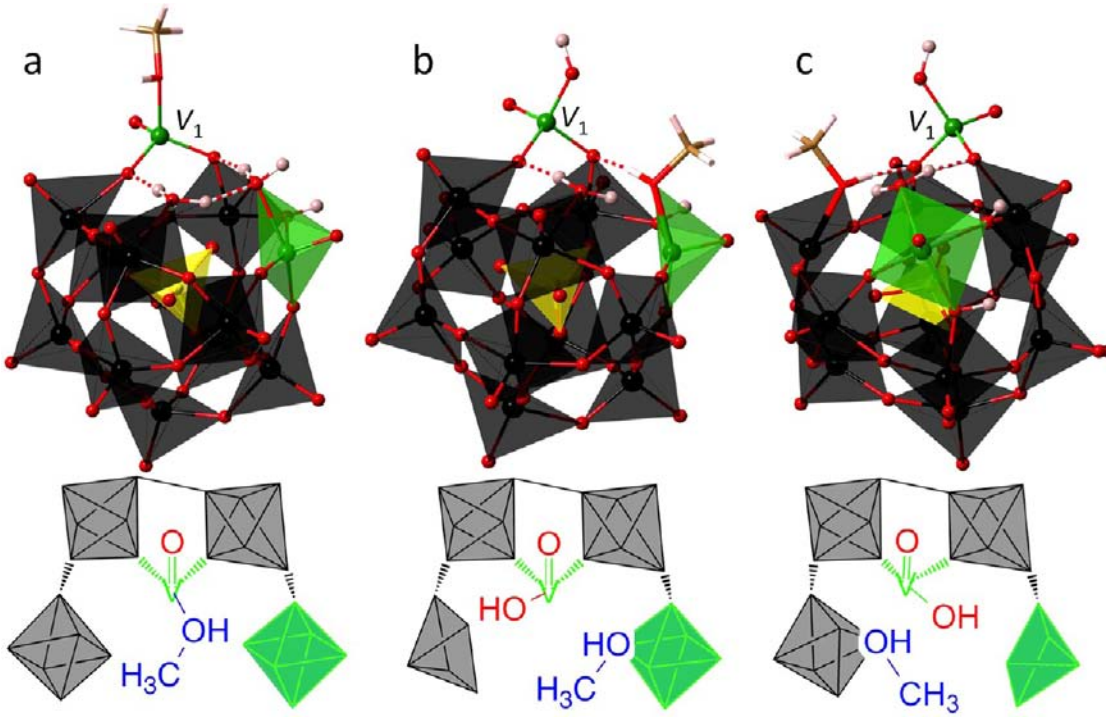

Figure 5. Coordination of a methanol molecule (shown in the tube model) on the displaced vanadium atom (a), and on dangling bonds of vanadium (b) and molybdenum (c) atoms within Keggin structure with the ***def*** $_2$ metal defect. For clarity, the interaction between the defect site and the substrate is schematically shown in the respective bottom panels.

total thermodynamic effect of the interactions (*vide infra*). Calculated energies of the representative ***def*** $_2$-XH and ***def*** $_2$-X complexes with substrates bound to the displaced vanadium atom in the gas phase and in acetonitrile solution are listed in Table S3 in the Supporting Information. For several substrates we considered CUSs on vanadium and molybdenum atoms within the Keggin structure as possible coordination sites in addition to the displaced vanadium atom. These complexes are included in Figures 3 and 4, if they are lower in energy. From Figures 3 and 4 one can see that different substrates exhibit diverse behavior not only at the initial stage of interaction but also in formation of intermediates and final products. Below we will discuss specific features of each reaction in more detail.

Activation of Alcohols. Displacement of vanadium atoms was observed *in situ* by molecular spectroscopy during the interaction of methanol with vanadium-containing molybdophosphoric acid in the gas phase at elevated temperatures.[5] It was found that methanol adsorption takes place within the Keggin structure as well as on the displaced VO_x units. Both VO_x sites in the primary Keggin structure and on the surface were significantly more active in methanol oxidation than the MoO_x sites. Calculated thermodynamic effects of the observed reactions 1a−1c show that, in the gas phase, methanol dehydrogenation by $H_5PV_2Mo_{10}O_{40}$ is energetically preferred to dehydration and that transfer of a second hydrogen atom to the reduced $H_6PV_2Mo_{10}O_{40}$ complex is preferred to the hydrogen transfer to a second polyoxometalate molecule in the oxidized state.

$$CH_3OH + H_5PV_2Mo_{10}O_{40} \xrightarrow{\Delta G_{298}=-13.3} H_2C{=}O + H_7PV_2Mo_{10}O_{40} \quad (1a)$$

$$CH_3OH + 2H_5PV_2Mo_{10}O_{40} \xrightarrow{\Delta G_{298}=-10.1} H_2C{=}O + 2H_6PV_2Mo_{10}O_{40} \quad (1b)$$

$$2CH_3OH \xrightarrow{\Delta G_{298}=-4.4} H_3COCH_3 + H_2O \quad (1c)$$

The high energies of proton and/or electron transfers, Table 1, make outer-sphere activation of methanol improbable. Indeed, even for CPET, the most energetically favorable outer-sphere reaction, the consequent transformation of complex **4**, is prohibitively high in energy, Figure 4. Thus, methanol activation should involve defect isomers of complex **1**. The O−H bond cleavage appears to be preferable to C−H bond cleavage; thus, methanol is coordinated by V−OR bonding. In agreement with the experimental results, we found that methanol could adsorb as nondissociated species on the displaced vanadium atom (V_1 in Figure 1c) or on CUSs formed on molybdenum and vanadium atoms in a ***def*** $_2$ structure (Figure 5) with energy costs of 24.3, 5.4, and 3.6 kcal/mol in the gas phase, respectively. Dissociation of the CH_3O−H bond—the obligatory step in both dehydration and dehydrogenation reactions—is exergonic by 20.8 kcal/mol for the displaced vanadium atom, isoenergetic for the CUS on the vanadium atom within the Keggin structure, and endergonic by 1.8 kcal/mol for the molybdenum site. Similar to water, ***def*** $_3$-methanol structures are energetically less favorable (ΔG_{298} = 20−21 kcal/mol in gas phase) and are perhaps the intermediates leading to further vanadium−oxygen bond cleavages. The ***def*** $_1$-methanol structures are also higher in energy than ***def*** $_2$, with ΔG_{298} = 18−20 kcal/mol for nondissociative coordination in the gas phase. They are more stable in the presence of an additional water molecule; however, taking into account the anhydrous conditions used for oxidative dehydrogenation of methanol and reaction temperatures above

dx.doi.org/10.1021/ja308625q | J. Am. Chem. Soc. 2012, 134, 20669−20680

200 °C, these complexes could be excluded from consideration of the reaction mechanism. Thus, at the reaction conditions, ***def*$_1$** and especially ***def*$_2$** complexes could serve as active forms of the catalyst. Although facile hydrogen transfer between the substrate and the adsorbent is most probable in such complexes (*vide supra*), consideration of the kinetics and mechanisms of the defect formation and consequent activity in methanol dehydration and oxidative dehydrogenation is needed for a complete representation of the reaction pathways of the concurrent reactions.

Higher alcohols show more complicated behavior upon interaction with $H_5PV_2Mo_{10}O_{40}$. Particularly, primary alcohols undergo atypical oxidation involving carbon−carbon bond cleavage rather than the usual oxidation at the α carbon to yield the corresponding aldehyde and then carboxylic acid.[4g] In our calculations, 1-butanol shows two coordination modes on the displaced vanadium atom V_1 of the ***def*$_2$** structure (Figure 1c). The first one, 5.7 kcal/mol uphill compared to the individual reagents in acetonitrile solution, is similar to the methanol coordination mode assisted by a dissociative O−H interaction. In the second, less favorable mode, coordination of the nondissociated 1-butanol molecule takes place via the three-center V−O−C_α bonding (25.2 kcal/mol higher in energy than the individual reagents), and the coordination center of the molecule further moves toward C_α in the presence of an additional water ligand. Additional study is needed in order to explore the detailed mechanism of the carbon−carbon bond cleavage reaction.

Oxidation of Ascorbic Acid. The most salient feature of the reduction of $H_5PV_2Mo_{10}O_{40}$ by ascorbic acid is displacement of a vanadyl VO^{2+} species from the Keggin structure that was observed by various EPR techniques in the reaction products at 20 and 140 K.[8a] It was found that the distance between the central P atom and the displaced V atom in this complex is larger than 5 Å and that the displaced V atom is bound to the parent polyoxometalate by only one bridging oxygen atom. However, the exact structure of this unique species could not be derived from the experimental data alone. Comparison between experimental and computational results sheds light on the nature of the experimentally observed complex and on the reason for its formation.

The dehydrogenation of ascorbic acid to dehydroascorbic acid, reaction 2a, is slightly exergonic, with an energy gain of 3.3 and 4.4 kcal/mol at 20 and 140 K, respectively. Dehydroascorbic acid is unstable, and its hydration, reaction 2b, yields diketogulonic acid.[39]

$$C_6H_8O_6 + H_5PV_2Mo_{10}O_{40} \xrightarrow{\Delta G_{140}=-4.4} C_6H_6O_6 + H_7PV_2Mo_{10}O_{40} \quad (2a)$$

$$C_6H_6O_6 + H_2O \xrightarrow{\Delta G_{140}=-3.7} C_6H_8O_7 \quad (2b)$$

Dehydrogenation of ascorbic acid by $H_5PV_2Mo_{10}O_{40}$ is not initiated by outer-sphere interactions, Table 1. Both ET and CPET reactions impede the formation of ***def*$_3$** and ***def*$_2$** complexes and consequent formation of adducts between activated ascorbic acid and ***def*$_2$** structures of $H_5PV_2Mo_{10}O_{40}$, Figures 3 and 4. Therefore, defect isomers of complex **1** present the most probable active form of the catalyst at the initial stage of interaction.

Ascorbic acid and its derivatives are known as either monodentate or O,O′-chelating ligands.[40] Particularly, vanadium complexes containing ascorbic acid as a monodentate ligand and the enol form of 2,3-diketogulonic acid as a bidentate ligand were isolated by Ferrer et al.[41] Very similar complexes could be found on the displaced vanadium atom of the ***def*$_2$** and ***def*$_1$** structures. Thus, a complex between ***def*$_2$**-$H_6PV_2Mo_{10}O_{40}$ and monodissociated ascorbic acid as a monodentate ligand is 5.1 and 1.4 kcal/mol downhill compared to the individual reagents at 20 and 140 K, respectively. In contrast, both ***def*$_2$**- and ***def*$_1$**-$H_7PV_2Mo_{10}O_{40}$ complexes with dehydroascorbic acid are much less stable (ΔG_{140} = +13.9 and +12.9 kcal/mol, respectively). Hydration of the coordinated dehydroascorbic acid to 2,3-diketogulonic acid dramatically stabilizes the interaction, so that its complex with ***def*$_2$**-$H_7PV_2Mo_{10}O_{40}$ (Figure 6a) becomes 23.1 and 13.7 kcal/mol lower in energy compared to the initial reactants at 20 and 140 K, respectively. Similarly, for VO^{2+} complexes it was shown that the primary complexes generated by the interaction of dehydroascorbic acid with metal ions are not stable and irreversibly hydrolyze to diketogulonic acid complexes.[41] Coordination of an extra water ligand causes cleavage of an additional V_1 bond to the Keggin structure, with formation of ***def*$_1$**-$H_7PV_2Mo_{10}O_{40}$ complex (Figure 6b) and additional stabilization of 10.2 and 4.5 kcal/mol at the two temperatures.

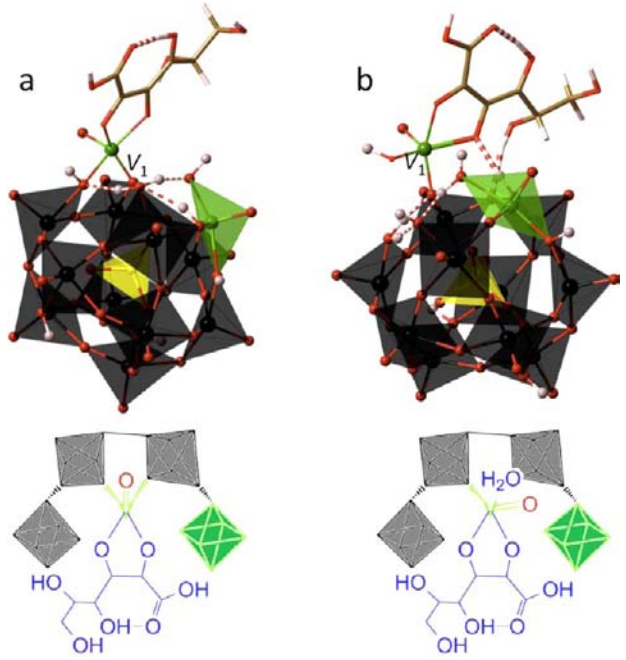

Figure 6. Stabilization of ***def*$_2$**- (a) and ***def*$_1$**-$H_7PV_2Mo_{10}O_{40}$ (b) complexes by the enol form of 2,3-diketogulonic acid (shown in the tube model) in the absence and in the presence of additional water ligand, respectively.

The characteristic V_1−P distances in these complexes are 4.5−4.8 and 5.1−5.3 Å, respectively, depending on the number and strength of hydrogen bonds around the displaced vanadium atom.[8] Notably, at low temperatures both complexes in Figure 6 are much more stable than intact $H_7PV_2Mo_{10}O_{40}$ and noncoordinated products dehydroascorbic or diketogulonic acid. For the most stable ***def*$_1$**-$H_7PV_2Mo_{10}O_{40}$ complex stabilized by the enol form of 2,3-diketogulonic acid and an additional water molecule, the calculated ΔG_{20} and ΔG_{140} are −33.3 and −18.2 kcal/mol. As a result, experimental identification of the most stable of them, the defect structure

dx.doi.org/10.1021/ja308625q | J. Am. Chem. Soc. 2012, 134, 20669−20680

in which vanadium atom is connected to the Keggin structure through a single oxygen bridge, became possible,[8a] and the experimentally estimated and theoretically predicted distances between the central P atom and the displaced V atom are in excellent agreement. Experimental identification of the metal defect complex in the reaction products at low temperatures implies that such structures could *a fortiori* serve as intermediates at other reaction conditions, such as stronger reducing agents and higher temperatures.

Oxidation of Anthracene and Xanthene. Reduction of $H_5PV_2Mo_{10}O_{40}$ by anthracene and xanthene as a stage in their selective oxidation by molecular oxygen was comprehensively studied using various experimental techniques.[4e] First, in strong support of our computational results, it was shown that protons are needed for the reaction to occur. Next, the experimental data suggest an outer-sphere ET as an initial step of the interaction. Accordingly, our calculations show that the outer-sphere ET from anthracene to $H_5PV_2Mo_{10}O_{40}$ is strongly exergonic (ΔG_{298} = −12.9 kcal/mol) and presents the only probable outer-sphere reaction channel (Table 1 and Figure 3). This is due to the high stability of polyaromatic cation radicals. Alkyl aromatic hydrocarbons typically show a lower propensity to stabilize an unpaired electron; thus, the outer-sphere ET from xanthene is less exergonic (ΔG_{298} = −3.8 kcal/mol), and the cation radical can undergo a proton transfer. Indeed, the outer-sphere CPET is only slightly (by 4.9 kcal/mol) higher in energy (Table 1 and Figure 4). Thus, the measured kinetic deuterium isotope effect on the initial step of the xanthene oxidation, k_H/k_D = 2.3 ± 0.08, can be attributed to CPET as a side reaction.

Experimentally, the anthracene cation radical was detected by EPR only in hexafluoroisopropanol as a solvent as a known stabilizer of cation radicals, whereas the xanthene cation radical was not detected even under these conditions. Moreover, the EPR spectrum of the paramagnetic $PV^{IV}V^{V}Mo_{10}O_{40}^{6-}$ indicated ion pairing between the reduced polyoxometalate and the anthracene cation radical. These observations led to the conclusion that the cation radicals form coordinated complexes with the polyoxometalate. Computationally, ion pairing between anthracene cation radical and $H_5PV_2Mo_{10}O_{40}^-$ destabilizes the **3**-***def*** $_2$ structure by an additional 16.8 kcal/mol, whereas electron pairing leads to the singlet complex, which is only 2.3 kcal/mol less stable than the **3**-***def*** $_2$ structure. Dissociation of the coordinated anthracene lowers the energy of the triplet complex by 4.0 kcal/mol and strongly destabilizes the singlet complex, Table S3. These energetic results identify facile formation of the ***def*** $_3$ and ***def*** $_2$ complexes followed by nondissociative anthracene coordination accompanied by electron pairing. In the resulting singlet complex the anthracene forms V_1−$C_{9(10)}$ bond of 2.28 Å in length, and the $C_{9(10)}$−H bond bends out of the plane of the aromatic ring by 164.6°, Figure 7a. The structure of this complex is consistent with a change of hybridization from sp^2 to sp^3 at the 9(10) aromatic carbon of anthracene, inferred from the kinetic isotope effect in the rate-determining step of the anthracene oxidation. The estimated reaction half-time for the formation of this complex, $\tau_{1/2}$ = 2.5 h at 60 °C in acetonitrile solution, is also consistent with the experimentally observed reaction rate. It is worth noting that, from steric considerations, the displaced V_1 atom represents the only possible coordination site for bulky anthracene and xanthene molecules in the ***def*** $_2$ structures.

Both the ET and CPET reaction channels lead to feasible inner-sphere xanthene coordination. As with anthracene, the initial ET step facilitates the formation **3**-***def*** $_3$ and **3**-***def*** $_2$ complexes following nondissociative xanthene coordination via V_1−O bonding assisted by electron pairing, Figure 3. The resulting complex, Figure 7b, is 18.1 kcal/mol above the individual intact **3** and xanthene cation radical and is easily accessible at the reaction temperature of 60 °C. The CPET reaction channel begins from benzylic C−H bond dissociation of xanthene followed by its coordination to a **4**-***def*** $_2$ structure via V_1−C bonding, Figure 7c. This stabilizes the defect species and is endergonic with respect to individual products of the outer-sphere CPET by 10.7 and 21.0 kcal/mol in the triplet and singlet states, respectively. Importantly, the inner-sphere proton transfer does not lead to mutual transformations of the **3**-***def*** $_2$-xanthene and **4**-***def*** $_2$-xanthene because of their different coordination modes. Therefore, the fact that further transformations of the **3**-***def*** $_2$-xanthene adduct along the ET reaction channel must include C−H bond cleavage imply a reaction pathway wherein the electron and proton have different donors and acceptors, in contrast to just hydrogen atom transfer implied in the CPET reaction channel. This mechanism often occurs in biochemical reactions.[31] The rational choice of the reaction mechanism of the xanthene oxidation requires determination of kinetic parameters and will be the topic of a separate communication.

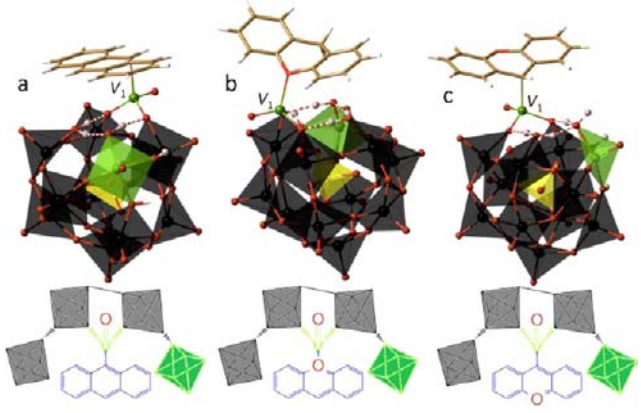

Figure 7. Nondissociative ***def*** $_2$-XH complexes of anthracene (a) and xanthene (b) and dissociative ***def*** $_2$-X(T) complex of xanthene (c). The substrates are shown in the tube model.

In strong support of the Mars−van Krevelen mechanism for aerobic anthracene and xanthene oxidations catalyzed by $H_5PV_2Mo_{10}O_{40}$, the oxygen transfer from the polyoxometalate to the substrate with formation of the experimentally observed products—anthraquinone and xanthen-9-one, respectively—is found to be energetically favorable. For anthracene, the total energy gain of reaction 3, ΔG_{298} = −17.1 kcal/mol in

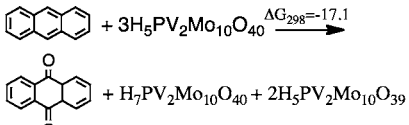

(3)

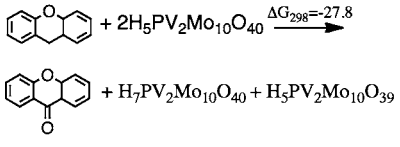

(4)

dx.doi.org/10.1021/ja308625q | J. Am. Chem. Soc. 2012, 134, 20669−20680

acetonitrile, is only 4.2 kcal/mol higher than that of the initial outer-sphere ET stage (ΔG_{298} = −12.9 kcal/mol). The total energetic effect of the xanthene oxidation reaction 4 is even more dramatic, ΔG_{298} = −27.8 kcal/mol, and much larger than that of the outer-sphere ET (−3.8 kcal/mol).

Oxidation of Thioanisole. Thioanisole presents the third substrate for which a low-temperature electron transfer−oxygen transfer mechanism was found experimentally.[4f] Another unique feature of the thioanisole oxidation under anaerobic conditions is the formation of a precipitate featuring the incipient formation of the sulfoxide and a VO^{2+} moiety supported on the polyoxometalate.[4f] Dissolution of this precipitate in CH_3NO_2 releases the sulfoxide product. Addition of O_2 also leads to the release of sulfoxide and regeneration of the initial $H_5PV_2Mo_{10}O_{40}$.[4f] Computationally, reaction 5a is

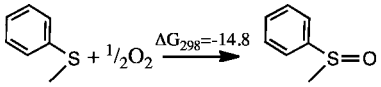

(5a)

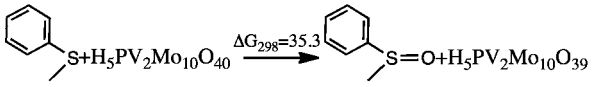

(5b)

exergonic (ΔG_{298} = −14.8 kcal/mol), but reaction 5b is strongly endergonic (ΔG_{298} = 35.3 kcal/mol); the oxygen transfer causes destabilization of the most stable ***def*$_2$**-thioanisole adduct by 24.9 kcal/mol. This suggests that dissolution of the experimentally observed precipitate with release of sulfoxide is a complex redox reaction and questions the validity of Mars−van Krevelen mechanism in this case.

Nevertheless, outer-sphere ET from thioanisole to $H_5PV_2Mo_{10}O_{40}$ is found to be exergonic in our calculations, Table 1. Subsequent coordination of thioanisole with formation of a V_1−S bond, Figure 8a, is prohibitively high in energy in the triplet state, although the singlet state of this complex is much more stable (with ΔG_{298} = 59.4 and 13.4 kcal/mol in acetonitrile, respectively). As in the case of methanol, thioanisole coordination to CUS on the vanadium atom within the Keggin structure (Figure 8b) is energetically more favorable and stabilizes the **3-*def*$_2$** structure by 8.2 and 10.3 kcal/mol in the triplet and singlet states, respectively. Outer-sphere CEPT at the initial stage of interaction is much higher in energy than ET for thioanisole, but still is possible at the reaction temperature of 70 °C. In this reaction thioanisole preferentially loses an aliphatic hydrogen atom and then is bound to the defect site by an aliphatic carbon atom. However, even if we assume that there exists a low-energy substrate-assisted pathway of defect formation, these complexes are much higher in energy than the above nondissociated ***def*$_2$**-thioanisole adducts, Figures 3 and 4. These results are in general agreement with the experimentally observed high selectivity of sulfoxide formation, indicating that the sulfur atom represents the most probable reaction center of the thioanisole molecule, as shown in Figure 8. The mechanism of thioanisole oxidation requires additional studies and should involve complexes with up to four coordinated thioanisole ligands, as suggested by the experiment.[4f]

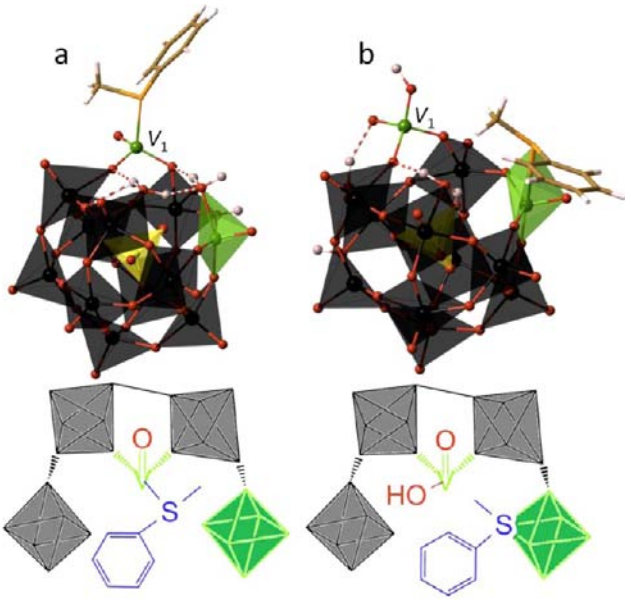

Figure 8. Thioanisole coordination on the displaced vanadium atom (a) and on the coordinatively unsaturated vanadium atom inside the ***def*$_2$** structure (b). The thioanisole ligand is shown in the tube model.

Oxidation of HI. Finally, we consider reduction of $H_5PV_2Mo_{10}O_{40}$ with HI as an illustrative redox reaction that demonstrates the importance of electron-transfer kinetics in H−X bond cleavage. From the thermodynamic viewpoint this reaction can proceed as an outer-sphere process, *vide supra*. In the gas phase, formation of a hydrogen bond, preferably with bridging O^{VV} and O^{V} atoms, precedes CPET, Figure S1 in the Supporting Information. In a polar solution, HI undergoes acidic dissociation followed by sequential protonation of the polyoxometalate and I^- coordination to one of the surface OH groups. Electron transfer is energetically favorable in such a system because of the relatively high stability of the iodine radical, Figure 9. An alternative reaction pathway involves

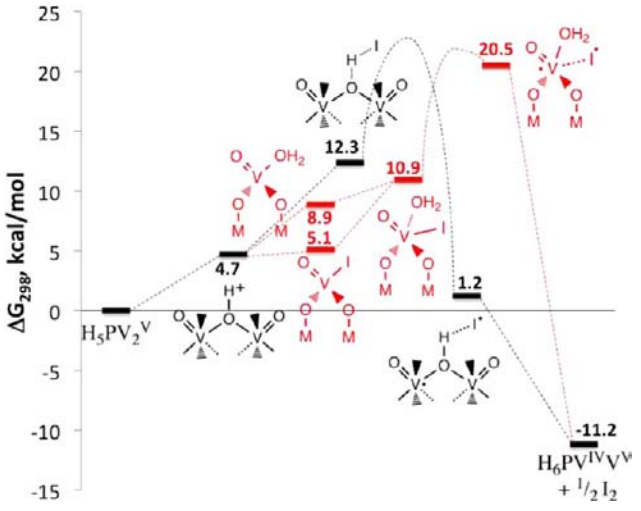

Figure 9. Thermodynamics of the outer-sphere (black) and inner-sphere (red) reduction of $H_5PV^V{}_2Mo_{10}O_{40}$ by HI in acetonitrile.

formation of a **2-*def*$_2$** structure assisted by coordination of I^- or water. Electron transfer in a ***def*$_2$**-I complex results in formation of a trigonal pyramid configuration about the displaced vanadium(IV) atom, which is energetically very unfavorable. In contrast, if both the iodide anion and water are coordinated to the displaced vanadium atom, the energetic cost for the electron transfer is 11.8 or 9.6 kcal/mol, respectively in the gas

dx.doi.org/10.1021/ja308625q | J. Am. Chem. Soc. 2012, 134, 20669−20680

phase or in acetonitrile. Thus, both reaction pathways are *thermodynamically* allowed at room temperature.

However, *kinetically* an electron transfer usually presents an activated process. Particularly, in solution it causes reorganization of the solvent net envelope, leading to a Franck−Condon barrier that is usually quite considerable.[42] In terms of Marcus theory,[43] the reorganization energy is determined by eq 6:

$$\lambda = K\left(\frac{1}{2a_1} + \frac{1}{2a_2} - \frac{1}{R}\right) \quad (6)$$

where a_1 and a_2 are ionic radii of the donor and acceptor, R is the distance the electron is transferred, and K is determined by the solvent properties and the amount of transferred electron density; $K \approx 330(1/\varepsilon_{op} - 1/\varepsilon_{st})$ kcal/mol, where ε_{op} and ε_{st} are the optic and static permeability of the solvent.[44] In the intermediate complexes for the outer-sphere and inner-sphere electron transfer shown in Figure 9, the V−I distances are 4.08 and 2.63 Å, respectively. Considering the ET as barrierless in the latter case,[45] the estimated activation energy for the long-range ET is about 22.5 kcal/mol.[46] More accurate calculation of the kinetic parameters of ET is the subject of a separate study, but here we stress that the mechanism of electron transfer is not unequivocal even for such a relatively simple reaction.

CONCLUSIONS

In the consensus Mars−van Krevelen oxygenation mechanism, the reaction is initiated by activation of a substrate through electron transfer from the substrate to the catalyst. This is followed by oxygen transfer from the reduced catalytic site to the activated substrate. Thus, the activity of the catalyst is usually correlated with its redox potential and its oxygen lability, whereas selectivity is usually controlled in catalysis by inner-sphere coordination of the substrate to a metal center. To complete the catalytic cycle, the reduced and deoxygenated catalyst can be regenerated by molecular oxygen. We have considered the details of the initial stages of substrate activation by a Mars−van Krevelen-type catalyst, $H_5PV^V_2Mo_{10}O_{40}$, using accurate quantum chemical calculations. The energetics of outer-sphere proton and electron transfer as well as coupled proton and electron transfer were calculated. This was followed by identification of possible key intermediates on the subsequent reaction pathways that involve CUSs of the previously unreported α-Keggin structures with *metal defects*. Gradual matching of the computational results with available experimental data for the wide variety of substrates considered in the present work shed light on the atomic-level understanding of the unique Mars−van Krevelen mechanism.

Proton-mediated formation of oxygen vacancies through the constitutional water loss presents the only surface defects previously considered in realistic charge-balanced DFT studies.[10,11] Although *displacement of metal atoms from the primary structure* is very likely in the Mars−van Krevelen mechanism, and numerous relevant experimental observations have been reported to this effect,[5,6,8] the geometry and electronic structure of metal surface defect species are generally unexplored. Previously, a defect structure with expansion of two adjacent five-coordinated metal atoms was reported as an intermediate in oxygen exchange in (Ge,Ga,Al)-Al_{12} ε-Keggin structures with positive charges of +7/8.[11c] Here we have presented three types of metal defects formed by protonation-induced cleavage of one, two, and three bridging metal−oxygen bonds that feature displacement of the metal atom from the Keggin structure with formation of several CUSs. The displacement is energetically more favorable for vanadium than for molybdenum atoms because of its higher ability to form low-coordinated oxo complexes that, in turn, could be traced back to the smaller size of its valence orbitals. The defect structures ***def***$_2$ and ***def***$_1$, with the displaced vanadium atom bound to the remainder of the Keggin structure by two or one bonds, respectively, are shown to be the most probable intermediates in most of the solution-phase redox reactions studied. Similar structures are suggested as active intermediates in oxygen isotope exchange reactions with water and in gas-phase methanol dehydrogenation. The defect structures with a five-coordinated metal atom are found to be much less energetically favorable.

For strong reducing agents, such as anthracene, xanthene, and thioanisole, the initial outer-sphere electron transfer, alone or possibly coupled with proton transfer for xanthene, facilitates formation of surface defects. Subsequent coordination allows for formation of reactive ensembles on the catalyst surface that are believed to be responsible for the selective oxygen-transfer step. The favorable energetics for the transfer of a bridging oxygen from the polyoxometalate surface to anthracene and xanthene provide theoretical support for the Mars−van Krevelen mechanism in these reactions. Weak reducing agents, such as primary alcohols and ascorbic acid, do not facilitate defect formation by outer-sphere electron and/or proton transfers, and thus formation of metal defect structures prior to the substrate activation is suggested here. In contrast to the metal catalysis, where hydrogen-atom transfer usually involves metal hydride formation, direct and virtually nonactivated H→O transfer takes place on the defect sites of oxide catalysts. The relevance of the metal defect structures as an active form of polyoxometalates in redox reactions is strongly supported by experimental observation of such structures in the products of $H_5PV_2Mo_{10}O_{40}$ reduction by ascorbic acid. The calculations show that this was possible because of the relatively low reduction potential of the substrate coupled with its strong complexation to the polyoxometalate at low temperature.

Water often has a critical influence on the performance of polyoxometalates in redox reactions. A small amount of water was shown to dramatically facilitate proton mobility in anhydrous polyoxometalates.[47] We have demonstrated that, in addition to this kinetic effect, traces of water strongly stabilize the reactive forms of polyoxometalates and also can serve as an essential constituent in the redox interaction. On the other hand, strongly bound water ligands can block CUSs from an incoming substrate.

The discussion here is based only on thermodynamic considerations. Substrates of various types that are oxidized by the Mars−van Krevelen mechanism are shown to follow various different reaction pathways, showing the diversity possible in such transformations. Further computational work is under way to explore the role of water and substrate coordination in defect formation, the mechanism of oxygen transfer and product formation, and related kinetic aspects including change of multiplicity and intersystem crossing.

ASSOCIATED CONTENT

Supporting Information

Full references, defect formation energies (ΔE and ΔG_{298} in gas phase, in water, and in acetonitrile) for the most stable structures, relative energies of the defect sites in gas phase, energies of representative ***def***$_2$-XH and ***def***$_2$-X complexes,

reaction profiles for reduction of $H_5PV^V_2Mo_{10}O_{40}$ by HI in gas phase, and optimized geometries and corresponding absolute energies of intact and defect complexes **1**−**4** and their adducts with adsorbed substrates. This material is available free of charge via the Internet at http://pubs.acs.org.

AUTHOR INFORMATION

Corresponding Author

ronny.neumann@weizmann.ac.il

Notes

The authors declare no competing financial interest.

ACKNOWLEDGMENTS

This research was supported by the Israel Science Foundation grant no. 1073/10, the Lise Meitner-Minerva Center for Computational Quantum Chemistry, and the Helen and Martin Kimmel Center for Molecular Design. R.N. is the Rebecca and Israel Sieff Professor of Chemistry. I.E. acknowledges financial support of the Center for Adsorption in Science, Ministry of Immigrant Absorption, State of Israel.

REFERENCES

(1) (a) *Polyoxometalate Molecular Science*; NATO Science Series II: Mathematics, Physics and Chemistry, Vol. *98*; Borrás-Almenar, J. J., Coronado, E., Müller, A., Pope, M. T., Eds.; Springer: Berlin, 2003. (b) *Polyoxometalate Chemistry: From Topology via Self-Assembly to Applications*. Pope, M. T., Müller, A., Eds.; Springer: Berlin, 2001. (c) Dey, K. C.; Sharma, V. *Int. J. ChemTech Res.* **2010**, *2*, 368−375.

(2) (a) Goloboy, J. C.; Klemperer, W. G. *Angew. Chem., Int. Ed.* **2009**, *48*, 3562−3564. (b) Hill, C. L. *Chem. Rev.* **1998**, *98*, 1−2.

(3) (a) Xu, L.; Boring, E.; Hill, C. L. *J. Catal.* **2000**, *195*, 394−405. (b) Neumann, R. *Prog. Inorg. Chem.* **1998**, *47*, 317−370. (c) Neumann, R.; Khenkin, A. M. *Chem. Commun.* **2006**, 2529−2538. (d) Neumann, R. *Inorg. Chem.* **2010**, *49*, 3594−3601.

(4) (a) Paul, S.; Le Courtois, V.; Vanhove, D. *Ind. Eng. Chem. Res.* **1997**, *36*, 3391−3399. (b) Benaissa, H.; Davey, P. N.; Khimyak, Y. Z.; Kozhevnikov, I. V. *J. Catal.* **2008**, *253*, 244−252. (c) Nakka, L.; Molinari, J. E.; Wachs, I. E. *J. Am. Chem. Soc.* **2009**, *131*, 15544−15554. (d) Khenkin, A. M.; Neumann, R. *Angew. Chem., Int. Ed.* **2000**, *39*, 4088−4090. (e) Khenkin, A. M.; Weiner, L.; Wang, Y.; Neumann, R. *J. Am. Chem. Soc.* **2001**, *123*, 8531−8542. (f) Khenkin, A. M.; Leitus, G.; Neumann, R. *J. Am. Chem. Soc.* **2010**, *132*, 11446−11448. (g) Khenkin, A. M.; Neumann, R. *J. Am. Chem. Soc.* **2008**, *130*, 14474−14476.

(5) Molinari, J. E.; Nakka, L.; Kim, T.; Wachs, I. E. *ACS Catal.* **2011**, *1*, 1536−1548.

(6) (a) Sultan, M.; Paul, S.; Fournier, M.; Vanhove, D. *Appl. Catal., A* **2004**, *259*, 141−152. (b) Jentoft, F. C.; Klokishner, S.; Kröhnert, J.; Melsheimer, J.; Ressler, T.; Timpe, O.; Wienold, J.; Schlögl, R. *Appl. Catal., A* **2003**, *256*, 291−317. (c) Ressler, T.; Timpe, O.; Girgsdies, F.; Wienold, J.; Neisius, T. *J. Catal.* **2005**, *231*, 279−291. (d) Watzenberger, O.; Emig, G.; Lynch, D. T. *J. Catal.* **1990**, *124*, 247−258. (e) Pacchioni, G.; Freund, H. *Chem. Rev.* **2012**, DOI: 10.1021/cr3002017.

(7) (a) Mestl, G.; Ilkenhans, T.; Spielbauer, D.; Dieterle, M.; Timpe, O.; Krohnert, J.; Jentoft, F.; Knozinger, H.; Schlögl, R. *Appl. Catal., A* **2001**, *210*, 13−34. (b) Jentoft, F. C.; Klokishner, S.; Krohnert, J.; Melsheimer, J.; Ressler, T.; Timpe, O.; Wienold, J.; Schlögl, R. *Appl. Catal., A* **2003**, *256*, 291−317. (c) Hodnett, B. K.; Moffat, J. B. *J. Catal.* **1984**, *88*, 253−263. (d) Brückner, A.; Scholz, G.; Heidemann, D.; Schneider, M.; Herein, D.; Bentrup, U.; Kant, M. *J. Catal.* **2007**, *245*, 369−380.

(8) (a) Kaminker, I.; Goldberg, H.; Neumann, R.; Goldfarb, D. *Chem.—Eur. J.* **2010**, *16*, 10014−10020. (b) Goldberg, H.; Kaminker, I.; Goldfarb, D.; Neumann, R. *Inorg. Chem.* **2009**, *48*, 7947−7952.

(9) (a) Pope, M. T.; Varga, G. M. *Inorg. Chem.* **1966**, *5*, 1249. (b) Creaser, I. C.; Heckel, M. C.; Neitz, R. J.; Pope, M. T. *Inorg. Chem.* **1993**, *32*, 1573. (c) Antonio, M. R.; Soderholm, L. *J. Alloys Compd.* **1997**, *250*, 541. (d) Liu, S.; Kurth, D. G.; Bredenkötter, B.; Volkmer, D. *J. Am. Chem. Soc.* **2002**, *124*, 12279. (e) Hill, C. L. Polyoxometalates: Reactivity. In *Comprehensive Coordination Chemistry II*; McCleverty, J. A., Meyer, T. J., Eds.; Pergamon: Oxford, 2003; pp 679−759. (f) Moffat, J. B. *Stud. Surf. Sci. Catal.* **1987**, *31*, 241−258. (g) Fernández, J. A.; López, X.; Bo, C.; de Graaf, C.; Baerends, E. J.; Poblet, J. M. *J. Am. Chem. Soc.* **2007**, *129*, 12244−12253.

(10) (a) Efremenko, I.; Neumann, R. *J. Phys. Chem. A* **2011**, *115*, 4811−4826. (b) For earlier calculations, see: Hirao, H.; Kumar, D.; Chen, H.; Neumann, R.; Shaik, S. *J. Phys. Chem. C* **2007**, *111*, 7711−7719.

(11) (a) Paul, J. F.; Founier, M. *Stud. Surf. Sci. Catal.* **2000**, *130*, 1199−1204. (b) Janik, M. J.; Bardin, B. B.; Davis, R. J.; Neurock, M. *J. Phys. Chem. B* **2006**, *110*, 4170−4178. (c) Rustad, J. R.; Loring, J. S.; Casey, W. H. *Geochim. Cosmochim. Acta* **2004**, *68*, 3011−3017. (d) Ohlin, C. A.; Villa, E. M.; Rustad, J., R.; Casey, W. H. *Nat. Mater.* **2010**, *9*, 11−19. (e) Casey, W. H.; Rustad, J. R.; Spiccia, L. *Chem.—Eur. J.* **2009**, *15*, 4496−4515. (f) Casey, W. H. *Chem. Rev.* **2006**, *106*, 1−16.

(12) (a) Frisch, M. J.; et al. *Gaussian 03*, Revision E.01; Gaussian, Inc.: Wallingford, CT, 2004. (b) Frisch, M. J.; et al. *Gaussian 09*, Revision B.01; Gaussian, Inc.: Wallingford, CT, 2009.

(13) (a) Kohn, W.; Sham, L. J. *Phys. Rev. A* **1965**, *140*, 1133. (b) Parr, R. G.; Yang, W. *Density Functional Theory of Atoms and Molecules*; Oxford University Press: New York, 1970; p 230.

(14) Perdew, J. P.; Burke, K.; Ernzerhof, M. *Phys. Rev. Lett.* **1996**, *77*, 3865−3868.

(15) (a) Jensen, F. *J. Chem. Phys.* **2001**, *115*, 9113−9125. (b) Jensen, F. *J. Chem. Phys.* **2002**, *116*, 7372−7379.

(16) Dolg, M. In *Modern Methods and Algorithms of Quantum Chemistry*; Grotendorst, J., Ed.; Neumann Institut für Computing: Jülich, 2000; Vol. *1*, pp 479−508.

(17) Martin, J. M. L.; Sundermann, A. *J. Chem. Phys.* **2001**, *114*, 3408−3420.

(18) (a) Dunlap, B. I. *J. Chem. Phys.* **1983**, *78*, 3140−3142. (b) Dunlap, B. I. *J. Mol. Struct. (Theochem)* **2000**, *529*, 37−40. (c) Nadykto, A. B.; Dua, H.; Yu, F. *Vibr. Spectrosc.* **2007**, *44*, 286−296.

(19) Khenkin, A. M.; Efremenko, I.; Weiner, L.; Martin, J. M. L.; Neumann, R. *Chem.—Eur. J.* **2010**, *16*, 1356−1364.

(20) Zhao, Y.; Truhlar, D. G. *J. Chem. Phys.* **2006**, *125*, 194101.

(21) (a) Jensen, F. *J. Chem. Phys.* **2002**, *117*, 9234−9240. (b) Jensen, F. *J. Chem. Phys.* **2003**, *118*, 2459−2463.

(22) (a) Klamt, A.; Schürmann, G. *J. Chem. Soc., Perkin Trans. 2* **1993**, 799−805. (b) Barone, V.; Cossi, M. *J. Phys. Chem. A* **1998**, *112*, 1995−2001.

(23) (a) Schwabe, T.; Grimme, S. *Phys. Chem. Chem. Phys.* **2007**, *9*, 3397−3406. (b) Schwabe, T.; Grimme, S. *Acc. Chem. Res.* **2008**, *41*, 569−579.

(24) Karton, A.; Tarnopolsky, A.; Lamère, J.-F.; Schatz, G. C.; Martin, J. M. L. *J. Phys. Chem. A* **2008**, *112*, 12868−12886.

(25) Siegbahn, P. E. M.; Blomberg, M. R. A.; Chen, S.-L. *J. Chem. Theory Comput.* **2010**, *6*, 2040−2044.

(26) Ryde, U.; Mata, R. A.; Grimme, S. *Dalton Trans.* **2011**, *40*, 11176−11183.

(27) Klamt, A. *Comput. Mol. Sci.* **2011**, *1*, 699−709.

(28) (a) Diaz, N.; Suarez, D.; Merz, K. M. *Chem. Phys. Lett.* **2000**, *326*, 288. (b) Rotzinger, F. P. *Chem. Rev.* **2005**, *105*, 2003. (c) Sadoc, A.; Messaoudi, S.; Furet, E.; Gautier, R.; Le Fur, E.; le Pollès, L.; Pivan, J.-Y. *Inorg. Chem.* **2007**, *46*, 4835−4843.

(29) See special issue devoted to reviews on Proton-Coupled Electron Transfer: *Chem. Rev.* **2010**, *110*, No. 12.

(30) Warren, J. J.; Tronic, T. A.; Mayer, J. M. *Chem. Rev.* **2010**, *110*, 6961−7001.

(31) Siegbahn, P. E. M.; Blomberg, M. R. A. *Chem. Rev.* **2010**, *110*, 7040−7061.

(32) Branytska, O. V.; Neumann, R. *J. Org. Chem.* **2003**, *68*, 9510−9512.
(33) In the intact $H_5PV^V_2Mo_{10}O_{40}$ complexes the P−V_1 distances vary from 3.52 to 3.69 Å.
(34) (a) Ilkenhans, T.; Herzog, B.; Braun, T.; Schlögl, R. *J. Catal.* **1995**, *153*, 275−292. (b) Pöppl, A.; Manikandu, P.; Köhler, K.; Maas, P.; Strauch, P.; Böttcher, R.; Goldfarb, D. *J. Am. Chem. Soc.* **2001**, *123*, 4577−4584. (c) Brückner, A.; Scholz, G.; Heidemann, D.; Schneider, M.; Herein, D.; Bentrup, U.; Kant, M. *J. Catal.* **2007**, *245*, 369−380.
(35) Mann, J. B. *Atomic Structure Calculations II. Hartree-Fock wave functions and radial expectation values: hydrogen to lawrencium*; LA-3691; Los Alamos National Laboratory: Los Alamos, NM, 1968.
(36) Casey, W. H.; Swaddle, T. W. *Rev. Geophys.* **2003**, *41*, 4-1−4-20.
(37) Rustad, J. R.; Casey, W. H. *Nat. Mater.* **2012**, *11*, 223−226.
(38) Duncan, D. C.; Hill, C. L. *J. Am. Chem. Soc.* **1997**, *119*, 243−244.
(39) Due to the entropic effect (one species forms two), this reaction becomes energetically more favorable at lower temperatures, with calculated ΔG_{20} = −8.4 kcal/mol.
(40) Zümreoglu-Karan, B. *Coord. Chem. Rev.* **2006**, *250*, 2295−2307.
(41) Ferrer, E. G.; Baran, E. *J. Biol. Trace Element Res.* **2001**, *83*, 111−119.
(42) (a) Kuznetsov, A. M. *Charge Transfer in Physics, Chemistry and Biology: Physical Mechanisms of Elementary Processes and an Introduction to the Theory*; Taylor & Francis: Oxford, UK, 1995. (b) Bu, Y.; Liu, Y.; Deng, C. *J. Mol. Struct. Theochem* **1998**, *422*, 219−228. (c) Weinstock, I. A. *Chem. Rev.* **1998**, *98*, 113−170.
(43) (a) Marcus, R. A. *J. Chem. Phys.* **1956**, *24*, 966−978. (b) Marcus, R. A. *J. Chem. Phys.* **1956**, *24*, 979−989. (c) Marcus, R. A. *Annu. Rev. Phys. Chem.* **1964**, *15*, 155−196.
(44) (a) German, E. D.; Kuznetsov, A. M. *Electrochim. Acta* **1981**, *26*, 1595−1608. (b) German, E. D. *Chem. Phys. Lett.* **1979**, *64*, 295−298. (c) German, E. D.; Kharkats, Yu. L. *Chem. Phys. Lett.* **1995**, *246*, 427−430.
(45) Shaik, S.; Danovich, D.; Fiedler, A.; Schröder, D.; Schwarz, H. *Helv. Chim. Acta* **1995**, *78*, 1393−1407.
(46) Structural data support the suggestion of significant Franck−Condon barriers in outer-sphere electron transfer. Indeed, optimized geometries of the outer-sphere HI complexes in the singlet and triplet states differ dramatically; the I→V electron transfer results in increased H−I distances from 2.24 and 2.22 to 2.52 and 4.26 Å, increased V−O distances from 1.96 and 1.94 to 2.01 and 1.97 Å, and decreased O−H distances from 1.04 to 0.97 and 1.00 Å, whereas APT charges significantly change not only on V (from 1.52 to 1.51) and I (from −0.22 to −0.03), but also on O (from −0.51 and −0.58 to −0.72 and −0.56) and H atoms (from 0.15 and 0.17 to 0.35 and 0.24). The inner-sphere electron transfer is accompanied by much smaller changes in geometry, with increasing V−I bond length of 0.14 Å and decreasing V−OH_2 bond length of 0.13 Å.
(47) Janik, M. J.; Davis, R. J.; Neurock, M. *J. Am. Chem. Soc.* **2005**, *127*, 5238−5245.